

Serial measurements of vascular permeability using bolus-tracking perfusion MR imaging in normal-appearing brain tissue following fractionated radiotherapy for glioma

M. C. Lee¹, J. Lupo¹, S. Cha¹, S. M. Chang², S. J. Nelson¹

¹Department of Radiology, University of California, San Francisco, CA, United States, ²Department of Neurological Surgery, University of California, San Francisco, CA, United States

1. Introduction

During external beam radiation therapy (XRT), significant doses of radiation are invariably delivered to healthy brain tissues. In this study, dynamic bolus tracking perfusion images (pMRI) were analyzed to study the dose-dependence and time-course of radiation-induced changes to brain vasculature following exposure to ionizing radiation. In previous studies, radioisotope flux studies and microscopy have been used in rat model systems to demonstrate microvasculature damage following high dose irradiation.¹ Using MRI, measurements of regional cerebral blood volume (rCBV) have suggested a decline in rCBV in normal-appearing tissues in the first year following radiation therapy.^{2,3} However, the calculation of rCBV requires assumptions regarding the shape of the perfusion time course, and so more direct analysis of vascular permeability may be better suited for studying radiation damage. In particular, leakage of contrast agent into the extravascular space results in the failure of the signal to return to pre-perfusion values. This study investigated the hypothesis that radiation effects in normal-appearing brain tissue could be measured by quantitative analysis of pMRI data and that pMRI derived vascular permeability would correlate with radiation dose.

2. Methods

Fourteen patients (8 female, 6 male, median age 49 ± 15) with a diagnosis of grade III (3 patients) or IV (11 patients) gliomas who were scheduled to receive fractionated XRT were recruited for this study. Each patient received a series of MRI exams on a 1.5 T Signa Echospeed scanner (GE Medical Systems, Milwaukee, WI) that were performed immediately before and after XRT and two months after the completion of radiotherapy. T2-FLAIR and T1-weighted SPGR images with and without gadopentetate dimeglumine (Gd-DTPA) contrast were acquired and used to exclude regions of T2 or T1-Gd abnormality from further analysis. Additionally, proton magnetic resonance spectroscopic imaging data was acquired using point resolved spectroscopy (PRESS) volume selection techniques using spectral-spatial spin-echo pulses, a TR/TE of 1000/144 ms. and a nominal voxel size of 1 cm^3 . Using a previously described automated abnormality quantification algorithm, voxels exhibiting an abnormal ratio of choline to *N*-acetylaspartate (NAA) were identified and excluded from further analysis.⁴ The perfusion imaging consisted of the injection of a bolus of 0.1 mmol/kg body weight of Gd-DTPA contrast agent at a rate of 5 mL/s. A series of 60 T2*-weighted echo-planar gradient-echo images were acquired before, during, and after the injection of the contrast agent, with a TR/TE of 1000/54 ms, 35° flip angle, a FOV of $26 \times 26 \text{ cm}^2$ with a 128×128 acquisition matrix, and a 3–6 mm nominal slice thickness. Prior to analysis, the perfusion series was resampled to a 32×32 grid in each plane. A mean of 1039 ± 392 voxels/exam/patient were then analyzed. The perfusion data series for each voxel was converted into relative $\Delta R2^*$ via the relationship $\Delta R2^*(t) \sim -\ln[S(t)/S_0]$, where S_0 was defined as the pre-injection baseline. The value of $\Delta R2^*$ was taken to be proportional to the concentration of contrast agent. The percent recovery for each voxel was defined as the difference between the peak value and the mean of the last five time points, expressed as a percent of the peak value. Dose distributions and CT volumes were aligned to the MRI images using normalized mutual information criteria, and the aligned doses were then resampled to the perfusion resolution.

3. Results and Discussion

Dynamic $\Delta R2^*$ curves for a patient at 2 months post-XRT are shown in figure 1, in which it can be seen that the shapes of the curves are similar between regions of the brain receiving different doses; however, the level of recovery differs between dose groups. The relationship between radiation dose to the percent recovery is shown in figure 2, in which recovery values have been normalized to the low dose voxels to highlight dose-dependent effects and suppress inter-patient variations. As expected, the pre-therapy values exhibit no difference between regions that will receive different doses, with all values within 1.2% of the low dose group. Immediately following therapy, no differences were found between any dose groups. However, 2 months following XRT, a significant dose-effect was observed, with an inverse relationship between the radiation dose and the percent recovery. Beyond 20 Gy, additional radiation dose only affected the level of recovery to a modest degree. In four of the five patients for which a two month follow-up was available, the inter-dose group differences were found to be statistically significant using Kruskal-Wallis non-parametric analysis of variance. Figure 3 shows the distribution of percent recovery values in regions receiving < 20 Gy and > 30 Gy, two months after XRT. The increased vascular permeability is reflected in the leftward shift of the histograms in the > 30 Gy region. The spatial distribution of these regions of incomplete recovery are shown in figure 4, in which the regions of with recovery between 50–75% are shown to be related to regions of higher dose.

4. Conclusions

A strong correlation between radiation dose and signal recovery during dynamic susceptibility-contrast imaging was found two months following the conclusion of fractionated radiation therapy. It is believed that this decreased recovery is suggestive of a small increase in microvascular permeability beyond the threshold of visibility on conventional T1-Gd imaging. These changes in perfusion imaging parameters may be useful in further understanding the degree and time course of radiation damage and repair in the central nervous system. Future studies will further increase the number of patients at each time point and investigate the long-term effects of damage to normal vasculature following radiation.

5. References

- [1] d'Avella *et al.* *Neurosurgery*. 30(1) 43–4 (1992).
- [2] Wenz F *et al.* *AJR Am J Roentgenol*. 166(1) 187–93 (1996).
- [3] Fuss *et al.* *Int J Rad Onc Biol Phys*. 48(1): 53–8 (2000).
- [4] McKnight *et al.* *J Magn Reson Imag*. 13(1): 167–77 (2001).

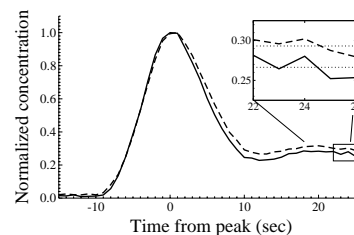


Figure 1. Dynamic concentration curves, normalized to peak height for one patient, 2 months post-XRT. Shown are 0–20 Gy (—) and 30–50 Gy (---). The recovery has been expanded to emphasize the difference between the dose groups.

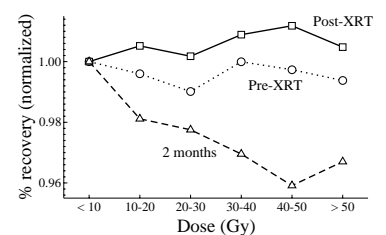


Figure 2. Normalized percent recovery as a function of dose prior to therapy (...), immediately after therapy (—), and 2 months post-therapy (---). All data were normalized to the low-dose value for the corresponding patient and time point.

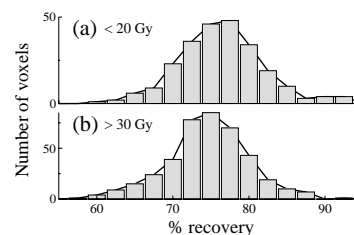


Figure 3. Histograms of percent recovery for a representative patient, taken two months after therapy. Shown are the (a) 0–20 Gy and (b) 30–50 Gy dose groups. The difference between the distributions was statistically significant using a Wilcoxon rank sum test.

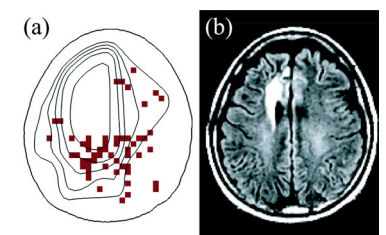


Figure 4. (a) A patient two months post XRT, highlighting voxels exhibiting 50–75% recovery (■). Voxels within the T2 or spectral abnormality have been suppressed. Also shown are the 20, 30, 40, 50, and 60 Gy isodose lines. (b) The T2-FLAIR image for the same slice.

This work was funded in part by grant P50 CA97297 from the NIH.